Volume 3 | Number 23 | 21 June 2015 | Pages 5871–6096

Journal of Materials Chemistry C

Materials for optical, magnetic and electronic devices

www.rsc.org/MaterialsC

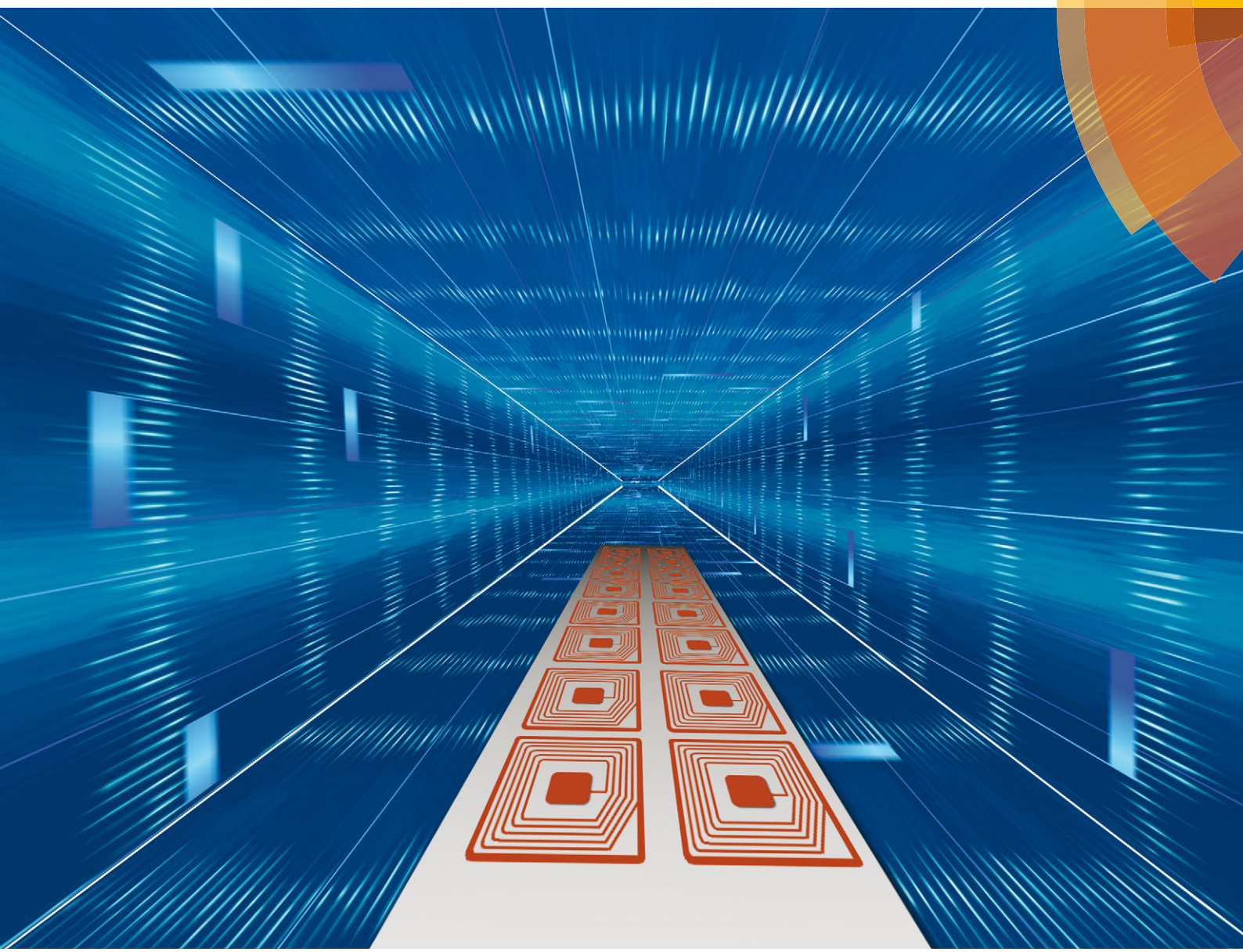

ISSN 2050-7526

ROYAL SOCIETY OF CHEMISTRY

PAPER

Tetsu Yonezawa *et al.*

The mechanism of alkylamine-stabilized copper fine particles towards improving the electrical conductivity of copper films at low sintering temperature

Journal of Materials Chemistry C

PAPER

View Article Online
View Journal | View Issue

Cite this: J. Mater. Chem. C, 2015, 3, 5890

The mechanism of alkylamine-stabilized copper fine particles towards improving the electrical conductivity of copper films at low sintering temperature†

Yingqiong Yong, Tetsu Yonezawa,* Masaki Matsubara and Hiroki Tsukamoto

Received 17th March 2015,
Accepted 8th April 2015

DOI: 10.1039/c5tc00745c

www.rsc.org/MaterialsC

To facilitate sintering of copper particles at low temperatures and achieve excellent electrical conductivity of copper films, reducing particle size is a common method. However, strong reducing agents which are usually used for reducing the size of particles limit their application. Here we report a novel approach to obtain highly conductive copper films. Firstly, copper fine particles were prepared by a one-pot reduction reaction utilizing D-isoascorbic acid as a mild reductant. Secondly, tight connection facilitating the sintering of particles was formed by generating convex surfaces, nanorods or nanoparticles during the oxidation procedure. The mechanism of the oxidative preheating process and its effects on the conductivity were clarified. High conductivity of copper films at low temperatures can be achieved due to the critical role of the oxidative preheating process.

Introduction

Printed electronics have attracted increasing attention due to their great potential in daily use.[1–4] As one of the printing techniques, inkjet printing[4] has become a particularly attractive method due to its simplicity, cost-efficiency, and on-demand performance. Metallic silver inks, which have the lowest resistivity and anti-oxidation properties in air,[5] have been widely used recently for printed electronics such as plastic electroluminescent devices and RFID tags.[6–8] However, silver inks cannot be used on a large scale because of their high cost and the low electromigration resistance of silver[5] which can result in circuit failure under high humidity conditions.

Copper inks, owing to the higher electromigration resistance of metallic copper,[9,10] much lower cost and low resistivity, have become a promising candidate for future conductive inks. In order to achieve high conductivity of copper films prepared from the copper inks, a well-known approach is to decrease the size of copper particles, which can facilitate the sintering of copper particles.[10–12] Generally speaking, strong reductants can produce nanoparticles because of their high nucleation rate and high density of nuclei.[13–15] Thus far, strong reductants such as hydrazine and sodium borohydride have been frequently utilized in the preparation of copper nanoparticles.[2,12,15–19] However, hydrazine is extremely dangerous and sodium borohydride can bring in impurities which are difficult to remove by a simple washing procedure using solvent.[20]

Instead of decreasing the size of nanoparticles to facilitate the sintering of copper particles, a facile thermal oxidation process which can increase the contact between particles might be another solution. Nanorods or nanowire-like coppper oxides prepared *via* a thermal oxidation process[21–24] have been extensively studied because of their wide range of applications in gas sensors,[25] heterogeneous catalysts,[26] *etc.* To our best knowledge, they have not been used for facilitating the coalescence of copper particles. Some reports have used an oxidative preheating process in air to remove the coated layers on copper nanoparticles[27] and demonstrated its crucial role in obtaining conductive films with a low resistivity.[28] However, the mechanism of the oxidative preheating process remains unclear. *In situ* TEM observation of copper fine particles with and without air can reveal the structural changes, but the complete understanding is still difficult.[27,29]

Herein, we propose a new route towards improving the conductivity using a mild reducing agent. This route can be achieved *via* a two-step process. Firstly, we synthesized copper fine particles by using D-isoascorbic acid[30–32] as the reductant and octylamine[33–36] as the capping agent. Then we successfully generated convex surfaces, nanorods or nanoparticles by an oxidative preheating process to facilitate the sintering of particles, resulting in excellent conductivity of copper films after sintering. To our best knowledge, the oxidative preheating process is demonstrated, for the first time, to facilitate the sintering of particles by generating

Division of Materials Science and Engineering, Faculty of Engineering, Kita 13 Nishi 8, Kita-ku, Sapporo, Hokkaido 060-8628, Japan. E-mail: tetsu@eng.hokudai.ac.jp; Fax: +81 011 706 7881; Tel: +81 011 706 7112

† Electronic supplementary information (ESI) available: Illustration of the detailed experimental process, data of copper **B** particles, and cross-sectional images of the copper **A** films, as well as XPD patterns after sintering. See DOI: 10.1039/c5tc00745c

nanorods or nanoparticles. The mechanism of the oxidative preheating process and its effects on the conductivity of copper films were studied. The results show that prepared copper films have high electrical conductivity due to the effects of the oxidative preheating process.

Experimental section

Synthesis of copper fine particles

The synthetic procedure used here is illustrated in Fig. 1. To prepare copper fine particles, we used cupric oxide (CuO, agglomerates with size ranging from a few hundred nanometers to several micro-meters, Nissin Chemco, Kyoto Japan) as the copper precursor, D-isoascorbic acid ($C_6H_8O_6$, 98%, Acros) as the reducing agent and octylamine (98%, Wako or Lion Corp., Japan) as the capping agent. The mixture of CuO (2.5 g, 31 mmol) and $C_6H_8O_6$ (5.5 g, 31 mmol), which was ground for 6 h by using a mortar, was dissolved in octylamine (52 cm^3, 310 mmol) in a two-neck round-bottom flask equipped with a magnetic stirring bar and a condenser. After 4 h stirring using a magnetic stirrer, the dispersing mixture was heated in an oil bath at 100 °C for 3 h at an agitation rate of 400 rpm. Then, the mixture was centrifuged and washed with ethyl acetate at 10 000 rpm for 30 min. The resulting precipitate was dispersed again into ethyl acetate by using sonication followed by centrifugation again. After carrying out the centrifugation process several times, the sample (copper **A**) was dried with a nitrogen flow. In addition, due to the low solubility of protonated octylamine[37] (some octylamine changed to protonated octylamine with the proton derived from ascorbic acid) in methanol, copper particles containing more protonated octylamine (copper **B**, detailed discussion in Fig. S2, ESI†) were also obtained using the same preparation method, followed by centrifugation using methanol three times and drying with a nitrogen flow.

Preparation of copper fine particle inks and films

For the preparation of copper **A** inks, synthesized copper **A** fine particles (30 wt%), which were ground using an automatic mortar for 30 min and pulverized using a blender for 4 min, were firstly dispersed into 70 wt% of α-terpineol (95%, Kanto, Japan). Ethanol, which was used for assisting redispersion of copper **A** fine particles and can be removed under reduced pressure, was added into the dispersion. Then, the α-terpineol dispersion of copper **A** fine particles was dispersed using a mixer for 32 min and using an emulsifier 5 times. At last, the copper **A** fine-particle inks were obtained by removing ethanol from the dispersion by evaporation under reduced pressure. The obtained copper **A** inks were deposited on aluminum oxide (Al_2O_3) (used for resistivity measurements) or on glass slides (used for X-ray diffraction (XRD) measurements) by a drop-coating method using a doctor blade, respectively. The thicknesses of sintered films at 200 °C, 250 °C and 300 °C were 4.4, 4.6, and 3.4 μm as shown in Fig. S3 (ESI†), respectively. After drying in nitrogen at 60 °C for 1 h, Al_2O_3 and glass slide substrates were cut into 2 cm × 2 cm pieces and annealed through a two-step process. In this two-step process, the substrates with copper **A** fine particle layers were heated at a flow rate of 2 dm^3 min^{-1} of air for 4 h and then sintered at a flow rate of 2 dm^3 min^{-1} of 3% hydrogen-containing nitrogen gas for 3 h (Fig. S1, ESI†). The temperature during annealing was kept at 200 °C, 250 °C or 300 °C. In addition, in order to investigate the morphological changes of the copper **A** fine particles during the oxidative preheating process, copper **A** films were heated at 200 °C and 250 °C at a flow rate of 2 dm^3 min^{-1} of air for various periods (5 min, 30 min, 2 h and 4 h) without sintering procedures.

Prepared copper **B** fine particles were also used for preparing the inks and films using the same method. Then, the prepared films were heated at 250 °C in air at the same flow rate for various oxidative preheating periods (5 min, 30 min, 2 h and 4 h).

Characterization

The crystal structures of facilely synthesized copper **A** fine particles and prepared copper **A** films were analyzed using XRD (Rigaku Mini Flex II, Cu Kα). The morphologies of the copper **A** fine particles and the copper **A** films were observed by using a field emission scanning electron microscope (FE-SEM, JEOL JSM-6701F) at an accelerated voltage of 15 kV. The thicknesses of the copper **A** films, which were used for calculating the volume resistivity of films were also measured using the cross-sectional SEM images of the obtained films. The sheet resistances of copper films were obtained using a four point probe method (Loresta-GP, MCP-T610, Mitsubishi Chemical Analytech, Japan).

For the copper **B** particles, thermal properties were measured by thermogravimetric analysis (TGA, Shimadzu DTG-60H). The films prepared using copper **B** particles were also characterized by XRD, SEM and resistivity measurements.

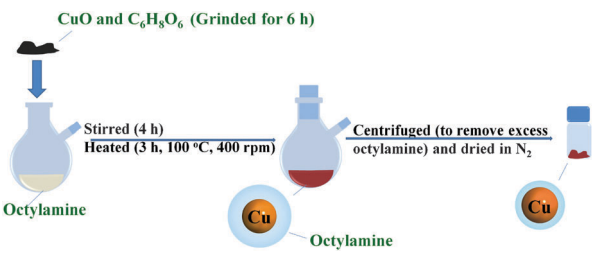

Fig. 1 Schematic illustration of the synthetic procedure of copper fine particles by a one-pot strategy.

Results and discussion

Copper fine particles were obtained by a one-pot process in the presence of octylamine (Fig. 1). SEM images and XRD patterns of copper **A** fine particles are displayed in Fig. 2. The size distribution of copper fine particles ranges from 130 nm to 330 nm with an average diameter of 280 nm, which was measured by calculating 100 particles statistically. The XRD pattern (Fig. 2b) shows five characteristic peaks at 43.3°, 50.4°, 74.1°, 89.9°, and 95.1°, which represent (111), (200), (220), (311), and (222) planes of copper crystallites, respectively. No peaks corresponding to copper oxides were detected. These can be attributed to the anti-oxidation role of octylamine. Amine is conducive to maintaining a reducing

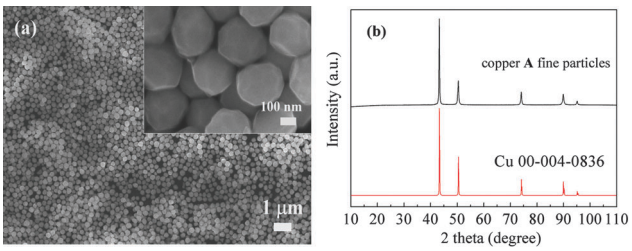

Fig. 2 (a) SEM images and (b) XRD patterns of copper **A** fine particles.

atmosphere during the reaction and preventing the oxidation of the particles by absorbing onto the surfaces of particles to form protective layers.[38,39] Recently, an inert atmosphere and strong reductants (*i.e.*, hydrazine,[2,15–19,27] sodium borohydride,[40] *etc.*) have been used for the preparation of copper fine particles and nanoparticles. In contrast, we synthesized copper fine particles using a mild reductant and an ambient atmosphere.

Fig. 3 shows SEM images and XRD of copper **A** films oxidatively preheated at 200 °C for various heating periods. Before the preheating process, copper **A** fine particles are separated by the organic layers. The surfaces of copper **A** fine particles are smooth (Fig. 3a), which indicates that no obvious oxidation of the particle surfaces occurred, which can also be confirmed by XRD patterns. At the preheating time of 5 min, convex surfaces and coalescence of particles can be obviously observed (Fig. 3b). With the increase of preheating time, coalescence of particles leads to tight connections between particles (Fig. 3b–e). According to the XRD analysis shown in Fig. 3f, there are apparent diffraction peaks of cuprous oxide (Cu_2O) besides those of metallic copper after the

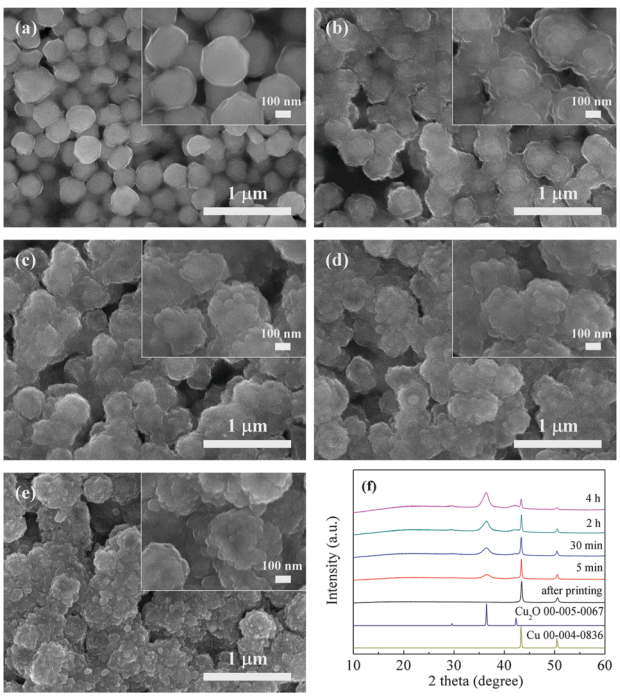

Fig. 3 SEM images of copper **A** films oxidatively preheated at 200 °C for various periods: (a) 0 min, (b) 5 min, (c) 30 min, (d) 2 h, and (e) 4 h. (f) Corresponding X-ray diffraction patterns.

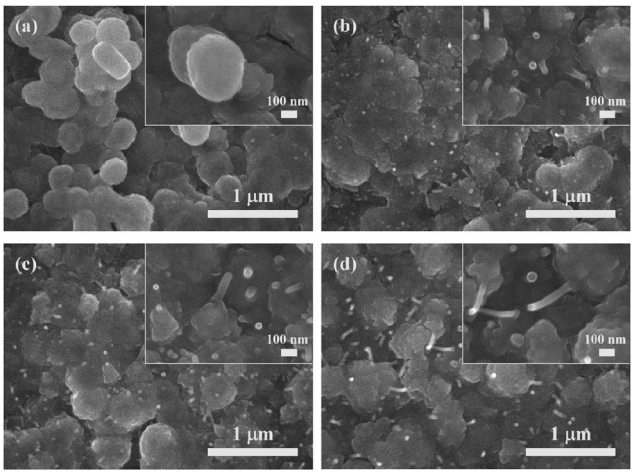

Fig. 4 SEM images of copper **A** films oxidatively preheated at 250 °C for various periods: (a) 5 min, (b) 30 min, (c) 2 h, and (d) 4 h.

oxidative preheating process, indicating that the convex surfaces are related to the generation of Cu_2O.

Fig. 4a–d show the SEM images of copper **A** films oxidatively preheated at 250 °C for various heating periods. With the increase of preheating time, convex surfaces and coalescence of some fine particles, which are the same as the results of copper **A** films oxidatively preheated at 200 °C, can also be observed (Fig. 4a–d). It should be noted that nanorods appeared besides the convex surfaces. The generated nanorods lead to the formation of denser films (Fig. 4b–d). XRD analysis of copper **A** films oxidatively preheated at 250 °C for various heating periods is shown in Fig. S4 (ESI†). Similar to the case of oxidative preheating at 200 °C shown in Fig. 3, copper fine particles started to be oxidized mainly to Cu_2O and small amounts of CuO at the preheating time of 5 min. With the increase of preheating time, the oxidation process continued with the decrease of intensity of metallic copper peaks. In combination with the results of SEM images (Fig. 4a–d), it can be concluded that the formation of copper oxides (Cu_2O or CuO) leads to the generation of convex surfaces at the beginning of the preheating process and nanorods as the oxidation procedure proceeds.

The other study in which copper **B** films were oxidatively preheated at 250 °C was also carried out. By contrast, their SEM and XRD results (Fig. 5a–f) show different results. Interestingly, what appeared on the convex surfaces in morphology was not nanorods but smaller nanoparticles (Fig. 5c–e). The XRD results exhibit that peaks representing metallic copper, Cu_2O and Cu_8O were detected at the preheating time of 5 and 30 min. Cu_8O, Cu_2O and CuO coexisted in the films oxidatively preheated for 2 and 4 h. Copper oxides have many forms, including well-known Cu_2O and CuO and other metastable phases (Cu_8O,[41] $Cu_{64}O$,[42] *etc.*). These metastable phases can be formed in the copper phase in certain depth during the atomic diffusion process.

The mechanism of the oxidative preheating process can be illustrated in Fig. 6. The main reactions during the oxidative preheating process can be explained by the following equations.

$$4Cu + O_2 \rightarrow 2Cu_2O \quad (1)$$

$$2Cu_2O + O_2 \rightarrow 4CuO \quad (2)$$

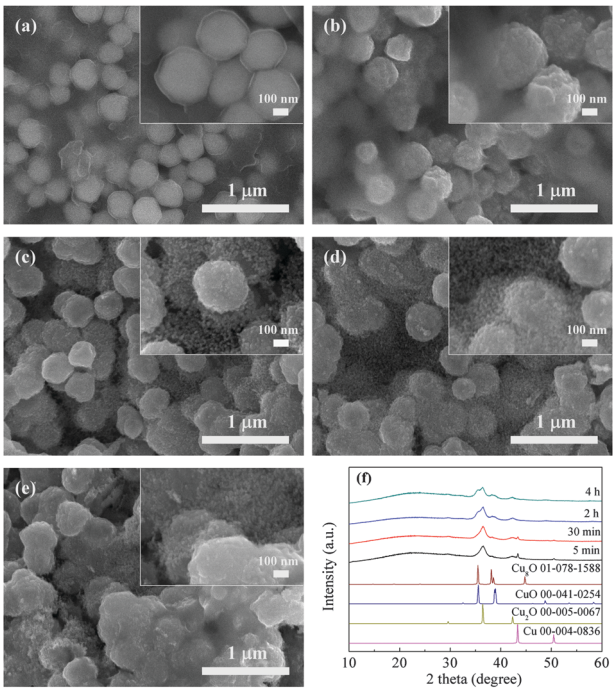

Fig. 5 SEM images of copper **B** films oxidatively preheated at 250 °C for various periods: (a) 0 min, (b) 5 min, (c) 30 min, (d) 2 h, and (e) 4 h. (f) Corresponding X-ray diffraction patterns.

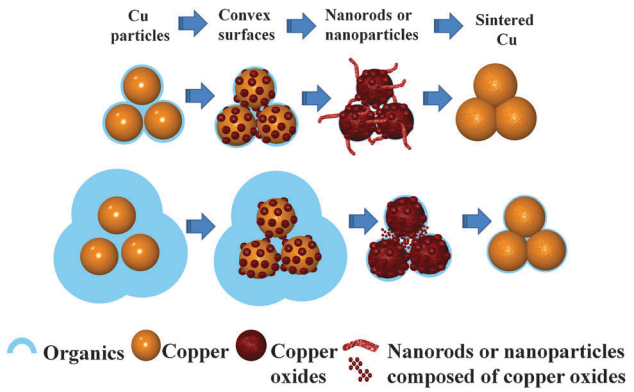

Fig. 6 Schematic illustration of the oxidation preheating process which can be used for generating convex surfaces, nanorods or nanoparticles and finally promote the sintering of particles.

The oxidation process involves copper ion diffusing from the copper matrix to the surface[22,43] and oxygen diffusion.[44] It can be divided into two stages. During the first stage, the diffusion of copper ions and oxygen results in the formation of convex surfaces (Fig. 3b–e, 4a and 5b). When the oxidative temperature is low, copper fine particles can only be oxidized to Cu_2O (eqn (1)). When the oxidative temperature is high enough, small amounts of formed Cu_2O as a catalyst can transform into a more stable CuO (eqn (2)).[23,45] If copper particles are surrounded by lots of protonated octylamine, the protonated octylamine may limit effective contact between copper ions and oxygen, which leads to the formation of Cu_8O which was found in XRD (Fig. 5f), and inhibits the generation of CuO. During the second stage, the growth of nanorods (Fig. 4b–d) or the formation of nanoparticles (Fig. 5c–e) happens. About the mechanism of nanorods or nanowires, it is often explained by the vapour–liquid–solid (VLS),[46] vapour–solid (VS),[47] or diffusion mechanism.[24,43] For the VLS mechanism, a catalyst is needed and droplets on the top of nanorods or nanowires are left. For the VS mechanism, our oxidative preheating process runs at low temperatures which are much lower than the melting point of copper and copper oxides.[22] The plausible reason for growth of nanorods might be that the local electric field established by the oxygen ions at the solid/gas interface enhances the diffusion of the copper ions[23] and reactions between copper ion and oxygen ions happen. This process during which reactions (1) and (2) take place simultaneously can only happen at a high oxidative temperature. If the copper particles are surrounded by plenty of protonated octylamine, the electrostatic force will interfere with the electric field. This interference may affect the diffusion of copper ions from the initial nuclear site to the tip of nanorods, resulting in the small nanoparticles. In addition, metastable Cu_8O, Cu_2O and CuO coexist in the films as a result of protonated octylamine.

Fig. 7 shows SEM images of copper **A** films preheated in air for 4 h (Fig. 7a, c and e) and copper **A** films annealed through a two-step process (Fig. 7b, d and f) at 200 °C, 250 °C and 300 °C, respectively. The morphologies of copper films oxidatively preheated at 200 °C, 250 °C and 300 °C for 4 h present that coalescence between particles took place significantly, leading to the formation of compact films. Moreover, the higher the preheating temperature was, the denser the obtained oxidative film

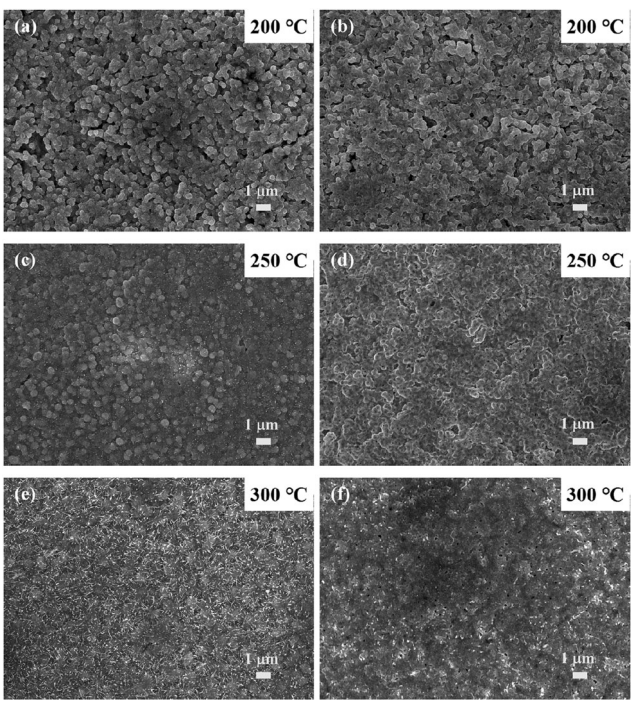

Fig. 7 SEM images of copper **A** films oxidatively preheated in air for 4 h (a, c and e) and copper films annealed through a two-step process which includes the oxidative preheating process in air for 4 h and reductive sintering in 3% hydrogen-containing nitrogen gas for 3 h at 200 °C, 250 °C and 300 °C, respectively (b, d and f).

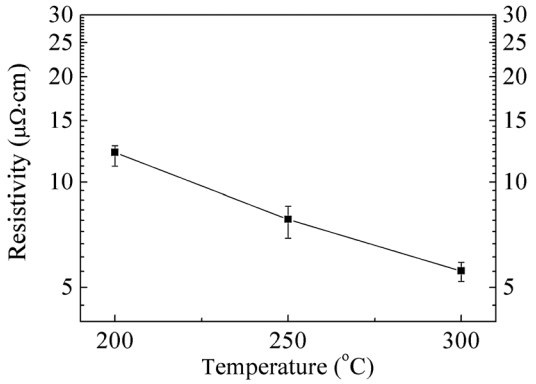

Fig. 8 Resistivity as a function of the annealing temperature of copper **A** films annealed through a two-step process.

was (Fig. 7a, c and e). After the reductive sintering process at various temperatures, the oxidative films were completely reduced to copper films (Fig. S5, ESI†) and highly dense copper films without obvious cracks were formed (Fig. 7b, d and f). And the copper film obtained at higher temperature became denser. Fig. 8 exhibits the resistivities of copper **A** films annealed through the two-step annealing process. The copper **A** films annealed at 200 °C, 250 °C and 300 °C exhibit excellent low resistivities of 12.2, 7.8 and 5.6 μΩ cm, respectively. The resistivity decreases as the annealing temperature increases, which is consistent with the SEM results in Fig. 7b, d and f. The resistivity of copper film annealed at 200 °C is only 7 times of that of bulk copper (1.7 μΩ cm). The outstanding electrical conductivity of annealed copper films can be attributed to the critical role of the oxidative preheating process. During the preheating process, generated convex surfaces are conducive to the tight connections between particles. Nanorods grow toward various directions, causing further connection of adjacent particles and formation of more compact network structures. Hence the sintering of particles was greatly facilitated. For copper **B** films, owing to the effects of small nanoparticles in the oxidative preheating process, these films which contain plenty of organics can also achieve relatively low resistivities of 82 and 86 μΩ cm at 250 °C and 300 °C, respectively (Fig. S6, ESI†). It is widely understood that small particles can facilitate the sintering of particles.[11,12] Furthermore, in our experiment, the produced nanoparticles lead to close contacts between particles and the formation of films with closely packed structure, which can promote the sintering of particles. Finally, after the reductive sintering process, sintered copper films with high conductivities can be obtained with the assistance of convex surfaces, nanorods or nanoparticles (Fig. 6).

It is generally recognized that the sintering process of copper particles takes place when the organic layers have been removed and the necks start to form between the particles.[11] Currently, most of the reports use the sintering process directly to remove the organic layers without carrying out the oxidative preheating process.[2,12,34] However, it is worth noting that the role of oxidative preheating is not only to remove the organic layers, but also to build close connections between particles and form highly compact films by the role of convex surfaces, nanorods or nanoparticles. Importantly, there are two advantages for using our method. Firstly, our method which uses copper fine particles can avoid or mitigate the problems caused by copper nanoparticles. The utilization of strong reductants can be avoided and copper fine particles are much easier to be stored than copper nanoparticles. As we know, the oxidation of copper nanoparticles under ambient conditions is severe, especially their size gets smaller. Secondly, in contrast with the method which needs to control the size of copper nanoparticles or form copper/silver core–shell nanoparticles[48] precisely and complicatedly, our thermal oxidation process is more facile and can also lead to excellent conductivity at low temperature.

Conclusion

In summary, a new route towards improving the electrical conductivity of copper film has been developed. This route, achieved through a two-step process, provides an effective method to form tight connections between particles by generating convex surfaces, nanorods or nanoparticles. Firstly, copper fine particles were synthesized using D-isoascorbic acid as a mild reductant and octylamine as a capping agent. Secondly, an oxidative preheating process in air was used for generating convex surfaces, nanorods or nanoparticles. The generation of convex surfaces, nanorods or nanoparticles during the oxidative preheating process is due to the diffusion of copper ions from the copper matrix to the surface and oxygen diffusion. The low resistivities of copper films can be ascribed to the role of the oxidative preheating process which promotes particle sintering. We expect that this facile route which overcomes some limitations of using copper nanoparticles would open up new possibilities for improving the conductivity of conductive films used for printed electronics.

Acknowledgements

This work is partially supported by Hokkaido University (to TY) and by Grant-in-Aid for Scientific Research (A) (to TY, 24241041) from JSPS, Japan.

Notes and references

1 T. Sekitani, H. Nakajima, H. Maeda, T. Fukushima, T. Aida, K. Hata and T. Someya, *Nat. Mater.*, 2009, **8**, 494–499.
2 D. Y. Deng, Y. R. Cheng, Y. X. Jin, T. K. Qi and F. Xiao, *J. Mater. Chem.*, 2012, **22**, 23989–23995.
3 S. Jeong, Y.-G. Ha, J. Moon, A. Facchetti and T. J. Marks, *Adv. Mater.*, 2010, **22**, 1346–1350.
4 M. Singh, H. M. Haverinen, P. Dhagat and G. E. Jabbour, *Adv. Mater.*, 2010, **22**, 673–685.
5 D.-H. Shin, S. Woo, H. Yem, M. Cha, S. Cho, M. Kang, S. Jeong, Y. Kim, K. Kang and Y. Piao, *ACS Appl. Mater. Interfaces*, 2014, **6**, 3312–3319.
6 S. Magdassi, M. Grouchko, O. Berezin and A. Kamyshny, *ACS Nano*, 2010, **4**, 1943–1948.

7 D.-Y. Shin, Y. Lee and C. H. Kim, *Thin Solid Films*, 2009, **517**, 6112–6118.
8 J. Perelaer, B.-J. de Gans and U. S. Schubert, *Adv. Mater.*, 2006, **18**, 2101–2104.
9 B. K. Park, D. Kim, S. Jeong, J. Moon and J. S. Kim, *Thin Solid Films*, 2007, **515**, 7706–7711.
10 G. Qin, A. Watanabe, H. Tsukamoto and T. Yonezawa, *Jpn. J. Appl. Phys.*, 2014, **53**, 096501.
11 C. Yang, C. P. Wong and M. M. F. Yuen, *J. Mater. Chem. C*, 2013, **1**, 4052–4069.
12 D. Y. Deng, Y. X. Jin, Y. R. Cheng, T. K. Qi and F. Xiao, *ACS Appl. Mater. Interfaces*, 2013, **5**, 3839–3846.
13 P. Lignier, R. Bellabarba and R. P. Tooze, *Chem. Soc. Rev.*, 2012, **41**, 1708–1720.
14 M. Chen, Y.-G. Feng, X. Wang, T.-C. Li, J.-Y. Zhang and D.-J. Qian, *Langmuir*, 2007, **23**, 5296–5304.
15 M. Tomonari, K. Ida, H. Yamashita and T. Yonezawa, *J. Nanosci. Nanotechnol.*, 2008, **8**, 2468–2471.
16 S. Jeong, H. C. Song, W. W. Lee, S. S. Lee, Y. Choi, W. Son, E. D. Kim, C. H. Paik, S. H. Oh and B.-H. Ryu, *Langmuir*, 2011, **27**, 3144–3149.
17 L. Q. Pham, J. H. Sohn, C. W. Kim, J. H. Park, H. S. Kang, B. C. Lee and Y. S. Kang, *J. Colloid Interface Sci.*, 2012, **365**, 103–109.
18 T. Yonezawa, N. Nishida and A. Hyono, *Chem. Lett.*, 2010, **39**, 548–549.
19 T. Yonezawa, Y. Uchida and Y. Abe, *J. Nanosci. Nanotechnol.*, 2014, **14**, 5402–5407.
20 Y. Zhang, P. L. Zhu, G. Li, T. Zhao, X. Z. Fu, R. Sun, F. Zhou and C.-P. Wong, *ACS Appl. Mater. Interfaces*, 2014, **6**, 560–567.
21 A. Li, H. H. Song, J. S. Zhou, X. H. Chen and S. Y. Liu, *CrystEngComm*, 2013, **15**, 8559–8564.
22 G. Filipič and U. Cvelbar, *Nanotechnology*, 2012, **23**, 194001.
23 Y. L. Liu, L. Liao, J. C. Li and C. X. Pan, *J. Phys. Chem. C*, 2007, **111**, 5050–5056.
24 X. Z. Li, J. Zhang, Y. W. Yuan, L. M. Liao and C. X. Pan, *J. Appl. Phys.*, 2010, **108**, 024308.
25 S. Deng, V. Tjoa, H. M. Fan, H. R. Tan, D. C. Sayle, M. Olivo, S. Mhaisalkar, J. Wei and C. H. Sow, *J. Am. Chem. Soc.*, 2012, **134**, 4905–4917.
26 Q. Zhang, H. Y. Wang, X. Jia, B. Liu and Y. Yang, *Nanoscale*, 2013, **5**, 7175–7183.
27 K. Ida, M. Tomonari, Y. Sugiyama, Y. Chujyo, T. Tokunaga, T. Yonezawa, K. Kuroda and K. Sasaki, *Thin Solid Films*, 2012, **520**, 2789–2793.
28 A. Yabuki and N. Arriffin, *Thin Solid Films*, 2010, **518**, 7033–7037.
29 T. Narushima, H. Tsukamoto and T. Yonezawa, *AIP Adv.*, 2012, **2**, 042113.
30 M. Ambrosi, P. Lo Nostro, E. Fratini, L. Giustini, B. W. Ninham and P. Baglioni, *J. Phys. Chem. B*, 2009, **113**, 1404–1412.
31 M. Del Bubba, E. Giordani, L. Pippucci, A. Cincinelli, L. Checchini and P. Galvan, *J. Food Compos. Anal.*, 2009, **22**, 668–677.
32 A. E. Karatapanis, Y. C. Fiamegos and C. D. Stalikas, *J. Sep. Sci.*, 2009, **32**, 909–917.
33 G. Salas, C. C. Santini, K. Philippot, C. Collière, B. Chaudret, B. Fenet and P. F. Fazzini, *Dalton Trans.*, 2011, **40**, 4660–4668.
34 S. Jeong, S. H. Lee, Y. Jo, S. S. Lee, Y.-H. Seo, B. W. Ahn, G. Kim, G.-E. Jang, J.-U. Park, B.-H. Ryu and Y. Choi, *J. Mater. Chem. C*, 2013, **1**, 2704–2710.
35 A. Yabuki, N. Arriffin and M. Yanase, *Thin Solid Films*, 2011, **519**, 6530–6533.
36 A. Yabuki and S. Tanaka, *Mater. Res. Bull.*, 2012, **47**, 4107–4111.
37 D. V. Talapin, J.-S. Lee, M. V. Kovalenko and E. V. Shevchenko, *Chem. Rev.*, 2010, **110**, 389–458.
38 Z. Xu, C. Shen, Y. Hou, H. Gao and S. Sun, *Chem. Mater.*, 2009, **21**, 1778–1780.
39 J. L. C. Huaman, K. Sato, S. Kurita, T. Matsumoto and B. Jeyadevan, *J. Mater. Chem.*, 2011, **21**, 7062–7069.
40 P. Pulkkinen, J. Shan, K. Leppänen, A. Känsäkoski, A. Laiho, M. Järn and H. Tenhu, *ACS Appl. Mater. Interfaces*, 2009, **1**, 519–525.
41 R. Guan, H. Hashimoto and K. H. Kuo, *Acta Crystallogr., Sect. B: Struct. Sci.*, 1984, **40**, 560–566.
42 R. Guan, H. Hashimoto and K. H. Kuo, *Acta Crystallogr., Sect. B: Struct. Sci.*, 1985, **41**, 219–225.
43 A. M. B. Gonçalves, L. C. Campos, A. S. Ferlauto and R. G. Lacerda, *J. Appl. Phys.*, 2009, **106**, 034303.
44 Z. Han, L. Lu, H. W. Zhang, Z. Q. Yang, F. H. Wang and K. Lu, *Oxid. Met.*, 2005, **63**, 261–275.
45 A. Yabuki and S. Tanaka, *Mater. Res. Bull.*, 2011, **46**, 2323–2327.
46 Y. Y. Wu and P. D. Yang, *J. Am. Chem. Soc.*, 2001, **123**, 3165–3166.
47 C. Liu, Z. Hu, Q. Wu, X. Z. Wang, Y. Chen, H. Sang, J. M. Zhu, S. Z. Deng and N. S. Xu, *J. Am. Chem. Soc.*, 2005, **127**, 1318–1322.
48 M. Grouchko, A. Kamyshny and S. Magdassi, *J. Mater. Chem.*, 2009, **19**, 3057–3062.